SPANDIDOS PUBLICATIONS

INTERNATIONAL JOURNAL OF MOLECULAR MEDICINE 39: 1173-1187, 2017

Effects of different cellulose membranes regenerated from *Styela clava* tunics on wound healing

SUNG HWA SONG[1], KEUM YONG SEONG[1], JI EUN KIM[1], JUN GO[1], EUN KYOUNG KOH[1], JI EUN SUNG[1], HONG JOO SON[1], YOUNG JIN JUNG[1], HYE SUNG KIM[2], JIN TAE HONG[3] and DAE YOUN HWANG[1]

[1]Department of Biomaterials Science, College of Natural Resources and Life Science/Life and Industry Convergence Research Institute, Pusan National University; [2]College of Nanoscience and Nanotechnology, Pusan National University, Miryang-si, Gyeongsangnam-do 627-706; [3]College of Pharmacy, Chungbuk National University, Cheongju, Chungbuk 361-763, Republic of Korea

Received November 6, 2015; Accepted February 23, 2017

DOI: 10.3892/ijmm.2017.2923

Abstract. The aim of this study was to investigate the therapeutic effects of three different cellulose membranes (CMs) manufactured from *Styela clava* tunics (SCTs) on the healing of cutaneous wounds. We examined the physical properties and therapeutic effects of three CMs regenerated from SCTs (referred to as SCT- CMs), including normal CM (SCT-CM), freeze-dried SCT-CM (FSCT-CM) and sodium alginate-supplemented SCT-CM (ASCT-CM) on skin regeneration and angiogenesis using Sprague-Dawley (SD) rats. FSCT-CM exhibited an outstanding interlayered structure, a high tensile strength (1.64 MPa), low elongation (28.59%) and a low water vapor transmission rate (WVTR) compared with the other SCT-CMs, although the fluid uptake rate was maintained at a medium level. In the SD rats with surgically wounded skin, the wound area and score of wound edge were lower in the FSCT-CM-treated group than in the gauze (GZ)-treated group on days 3-6 and 12-14. In addition, a significant attenuation in the histopathological changes was observed in the FSCT-CM-treated group. Furthermore, the expression level of collagen-1 and the signaling pathway of transforming growth factor (TGF)-β1 were significantly stimulated by the topical application of FSCT-CM. However, no signs of toxicity were detected in the livers or kidneys of the three SCT-CM-treated groups. Overall, our data indicate that the FSCT-CM may accelerate the process of wound healing in the surgically wounded skin of SD rats through the regulation of angiogenesis and connective tissue formation without inducing any specific toxicity.

Correspondence to: Professor Dae Youn Hwang, Department of Biomaterials Science, College of Natural Resources and Life Science/Life and Industry Convergence Research Institute, Pusan National University, 50 Cheonghak-ri, Samnangjin-eup Miryang-si, Gyeongsangnam-do 627-706, Republic of Korea
E-mail: dyhwang@pusan.ac.kr

Key words: cellulose membrane, wound dressing, *Styela clava* tunics, collagen, transforming growth factor-β

Introduction

Medical dressings have been widely applied in the treatment of external cutaneous wounds, such as abrasions, lacerations, avulsions, puncture wounds, contusions, blisters, incisions, burns, split graft donor sites and ulcers (1). Among the many properties of dressings, the water vapor transmission and water retention properties are considered key factors for regulating the moisture balance in the wound area (2). Specifically, these factors should provide a moderate atmosphere by transpiring excess exudates promptly and retaining adequate moisture to promote tissue regeneration (3). To satisfy the above conditions of dressings, a versatile class of polymers has been extensively applied as their flexibility during synthesis or modification of polymers can enable the matching with the physical and mechanical properties of various tissues or organs in the human body (4). Among these, polymers with good physical, mechanical and chemical properties have been investigated as substrates for wound healing (5). Polyurethane (PU) is frequently applied to wound dressings due to its good barrier properties and oxygen permeability, while chitin/chitosan have shown positive effects on wound healing as they are biocompatible, biodegradable, non-toxic, anti-microbial and hydrating agents (6,7). Moreover, hydrated hydrogel sheets have shown good coherency, transparency, flexibility, high oxygen permeability and good skin adhesion (8), whereas non-woven fabrics can be readily conditioned to serve as an excellent dressing material as they contain high porosity and a large surface area with no dust, are easily processable and have a readily modifiable surface mechanism (9).

Various types of cellulose have been extensively applied to the treatment of skin wounds as part of the development of new materials. Crystalline cellulose membranes (CMs) have been directly applied to the skin wounds of Wistar rats for 26 days to evaluate the effects on healing. These membranes contribute to the maintenance of the humidity of the wound, decrease pain, and ease the visualization and control of the evolution of the

lesion (10). The hydrocolloid membrane cellulose containing *Styela clava* tunic (SCT) powder (HCM-SCT) has been shown to accelerate the repair process of acute wounds in Sprague-Dawley (SD) rats through the stimulation of re-epithelization, collagen deposition and angiogenesis (11). Furthermore, the oxidized regenerated cellulose (ORC) collagen has been shown to significantly stimulate diabetic wound closure, resulting in a measurable improvement in the histological appearance of wound tissue (12). In our previous studies, cellulose film was successfully prepared using pure cellulose powder obtained from SCTs after completing dissolution in *N*-methylmorpholine-*N*-oxide (NMMO)/H_2O (87/13 wt%) (13) or [Amim]Cl ionic liquid composed of 1-methylimidazol and 3-chloro-1-propene (14). This film exhibited good biocompatibility and degradability, as well as a therapeutic effect on the wounded skin of SD rats (14,15). However, there have been no attempts to date (to the best of our knowledge) to develop and invest in novel membranes with enhanced porosity to promote the repair of surgical wound skin.

In the present study, we compared skin regeneration and angiogenesis in the surgical wounds of SD rats after the application of three different SCT-CMs for 14 days. The results of the present study provide novel evidence that FSCT-CM may be considered as a wound dressing material which may be used to accelerate the process of wound healing in the injured skin of SD rats through the regulation of angiogenesis and connective tissue formation.

Materials and methods

Preparation of three SCT-CMs. SCT powder was prepared as previously described (14). Briefly, to remove sediments and debris, 33 g of SCTs in 10% NaOH aqueous solution (990 ml) were boiled at 100˚C for 2 h after being collected from the beach of the South Sea in Gosung-gun, Korea. The SCT samples were subsequently washed with distilled water 3 times, after which they were boiled in 5% CH_3COOH solution at 100˚C for 2 h to neutralize the NaOH solution, then washed with distilled water 3 times. SCT was subsequently bleached by separate boiling and washing in 10% H_2O_2 solution. After a final wash with distilled water, SCT was dried at 100-120˚C for 2-3 h, then ground in a pin mill machine (Daehwa, Yongin, Korea). The milling for SCT powders was conducted by a proprietary commercial process consisting of passing through a combination of 30 mesh sieves for 10 min once, and then 120 mesh sieves for 10 min 2 times.

Three types of SCT-CMs were also prepared using a modified version of the method described in a previous study (14). To manufacture SCT-CM (the first type), 3 g of SCT powder was completely dissolved in 100 ml of [Amim]Cl ionic liquid composed of 1-methylimidazole and 3-chloro-1-propene (1:1.20 of molar ratio) at 80˚C. Additionally, another cellulose solvent, *N*-methyl-2-pyrrolidone (NMP) was added followed by stirring at a high speed for 24 h to accelerate the dissolution of SCT. These solutions were then cast onto the glass plate of an automatic film coating apparatus (DAO-CO 02; Dao Technology, Hwaseong, Korea) to yield a thickness of approximately 3 mm. Following the removal of air bubbles under a vacuum oven, the glass plates bound with CM were immediately immersed in methanol and washed with distilled water. Finally, CMs with a thickness of approximately 3 mm were collected by drying at room temperature for 24 h. FSCT-CM (the second type of CM) was prepared from SCT-CM through dehydration in a lyophilizer (FDU-540; Tokyo Rikakikai Co., Tokyo, Japan) following incubation at -130˚C for 24 h. Furthermore, to prepare ASCT-CM (the third type of CM), SCT powder was completely dissolved in 100 ml of 8% sodium alginate solution (Sigma-Aldrich Co., St. Louis, MO, USA) with 0.976 g/ml. Following immersion in 10% (w/v) $CaCl_2$ solution for 24 h, these composites were cast onto the glass plate of an automatic film coating apparatus to give a thickness of approximately 3 mm. Following the removal of air bubbles under a vacuum oven, the glass plates bound with CM were immediately immersed in methanol and washed with distilled water, after which CMs with a thickness of approximately 3 mm were collected by drying at room temperature for 24 h.

Finally, the three different types of SCT-CMs in our study were prepared as membranes with 70% moisture content by dipping in 1X phosphate-buffered saline (PBS) solution immediately before application onto the skin of SD rats. Gauze (GZ) used as a negative control was prepared under the same conditions after sterilization.

Analysis of the physical properties of the three SCT-CMs. To analyze the morphological features of the three SCT-CMs, samples were frozen at -70˚C for 24 h, after which they were dehydrated in a lyophilizer for 3 days. These dried SCT-CMs were then coated with platinum (Pt) using a sputter coater (Jeol JXA-840A; Jeol, London, UK) for 120 sec under an argon atmosphere, after which they were observed by scanning electron microscopy (SEM) (Stereoscan 250 MK III; Cambridge Instruments, London, UK) at 15 kV. After capturing the SEM image, the gap length and the pore diameter in inside of SCT-CMs was measured using Leica Application Suite (Leica Microsystems, Wetzlar, Germany).

The mechanical properties, including tensile strength, elongation, fluid uptake rate and water vapor transmission rate (WVTR) of the three SCT-CMs were measured by the methods described in a previous study (14). To perform the tensile strength and strain analysis, the three SCT-CMs were dried at 105˚C for 12 h and then cut to an appropriate size (1x5 cm). Two properties of these samples were analyzed (40 kV, 30 mA) at room temperature under a velocity of 20 mm/min using a United SSTM-1 testing machine (United Calibration Corp., Huntington Beach, CA, USA) with a 445 N load cell.

Additionally, the swelling behavior of the three SCT-CMs (1x5 cm size) was investigated by the immersion in 30 ml of 1X PBS (pH 7.4) at 37˚C. At 7 time points (0.167, 0.5, 2, 4, 8, 16 and 24 h) after the immersion, each sample was removed from the solution, the excess of water at surface withdrawn and their weight immediately determined. The fluid uptake rate was the calculated using the following equation, as previously described (16): fluid uptake rate (%) = $[(W_o - W_i)/W_i)$ x100], where, W_o and W_i represent the wet and dry weight of the film, respectively. Five samples were used for each condition.

Furthermore, to determine the moisture permeability of the three SCT-CMs, the WVTR was measured according to the American Society for Testing and Materials (ASTM) standard (17). Each sample from the three SCT-CMs was cut into a disc with a diameter of 50 mm and mounted on the mouth of

a cylindrical cup with a diameter of 40 mm containing 30 ml of water. The sample was placed into an oven (FO-600M; Jei Tech, Seoul, Korea) and maintained at 37±2˚C and 35±5% relative humidity. At 7 different time points (1, 2, 4, 8, 16, 24, 48 and 72 h) after the drying of the SCT-CMs began, their weight was immediately determined and the WVTR was then calculated using the following equation: WVTR (g/m^2/h) = [(W_i - W_t)/A/24) x10^6, where, W_i and W_t represent the weight of the initial time, the time 't' and the area 'A' at different periods of time. Five samples were repeatedly measured 3 times for each condition.

Design of animal experiment. The animal protocol used in this study was reviewed and approved by the Pusan National University-Institutional Animal Care and Use Committee (PNU-IACUC; approval no. PNU-2014-0520). Adult male SD rats were purchased from SamTako BioKorea (Osan, Korea) and handled at the Pusan National University Laboratory Animal Resources Center accredited by the Korea Food and Drug Administration (accredited unit no. 00231) and AAALAC International (accredited unit no. 001525). All rats were provided with a standard irradiated chow diet (Purina Mills, Seoungnam, Korea) *ad libitum*, and were maintained in a specific pathogen-free state under a strict light cycle (lights on at 06:00 h and lights off at 18:00 h) at a temperature of 23±2˚C and a relative humidity of 50±10%.

An *in vivo* wound healing assay was developed in which 7-week-old SD rats (n=40) were assigned to one of 4 groups as follows: a GZ-treated group (n=10); a SCT-CM-treated group (n=10); a FSCT-CM-treated group (n=10); and a ASCT-CM-treated group (n=10). Each group was then further divided into 2 different groups: 7 days (n=5) and 14 days (n=5). The animals were anesthetized by an intramuscular injection of Zoletile (50 mg/kg body weight) and Rompun (5 mg/kg body weight), after which the back skins were shaved with an electrical razor and 70% ethanol was applied. A round wound with a diameter of 8 mm and a depth of 2-4 mm was formed by removing the cutaneous tissue in the back shoulder region using a biopsy punch (Kasco Com, Sialkot, Pakistan). The incision wound on each rat was then sterilized with 70% ethanol, after which it was covered with a 5x4x0.3 mm piece of GZ, SCT-CM, FSCT-CM or ASCT-CM. The pieces of GZ and the three types of CMs were replaced with new pieces every 3 days. During replacement, the condition of the wound skin was observed and photographed using a Canon® digital camera, while the body weight was measured using an electronic balance (Mettler Toledo, Greifensee, Switzerland). On days 7 and 14, all rats were subjected to euthanasia using carbon dioxide, and samples of damaged skin were collected for further histological analysis and western blot analysis. Additionally, blood serum and liver and kidney organs were collected from the abdominal veins and the abdominal cavity to analyze the toxicity of the three SCT-CMs.

Macroscopic analyses of surgical wounds. Photographic data were utilized for the measurement of the wound size (%), which was calculated as follows:

$$\text{Wound size (\%)} = \frac{W_t}{W_0}$$

where W_t is the wounded area at time 't' and W_0 is the wounded area at the initial time. A multiple comparisons test was performed for the statistical clarification of the differences between groups. In addition, the analysis of wound color (1, red; 2, pink; 3, pale; 4, cyan) and wound edge (1, without granulation tissue; 2, little granulation tissue; 3, much granulation tissue) were scored as previously described (10).

Serum biochemistry. On days 7 and 14, all SD rats in each group were fasted for 8 h, after which blood was collected from the abdominal veins of rats and incubated for 30 min at room temperature. Serum was then obtained by the centrifugation of blood and serum biochemical components, including alkaline phosphatase (ALP), alanine aminotransferase (ALT), aspartate aminotransferase (AST), blood urea nitrogen (BUN), and creatinine (CRE) were assayed using an automatic serum analyzer (Hitachi 747; Hitachi, Tokyo, Japan). All assays were measured using fresh serum and conducted in duplicate.

Histological analyses. The skin in the region in which GZ and the three SCT-CMs had been placed was collected and fixed with 10% formalin for 48 h, embedded in paraffin wax, and then sectioned into 4-μm-thick slices. The skin sections were subsequently stained with hematoxylin and eosin (H&E; Sigma-Aldrich Co.), after which they were examined under a light microscope (Leica Microsystems) for the presence of edema and inflammatory cell accumulation. Additionally, the thickness levels of the epidermis, including the stratum germinativum (SG), stratum spinosum (SS) and stratum granulosum (SGR), as well as the number of neutrophils and macrophages (cells/0.16 mm^2 of field) and blood vessels (cells/1.4 mm^2 of field) were measured using Leica Application Suite (Leica Microsystems). In addition, the livers and kidneys collected from all experimental rats were processed using the same methods applied to treat the skin tissue. After staining with H&E, pathological changes in the liver and kidney sections were examined using Leica Application Suite (Leica Microsystems).

Mast cells in the skin sections were detected by staining with toluidine blue (Sigma-Aldrich Co.) as previously described (18). The number of cells per 0.01 mm^2 of observed field in skin tissue sections was then measured using Leica Application Suite (Leica Microsystems).

Western blot analysis. Skin tissue isolated from a subset of groups was homogenized using a PRO-PREP™ Solution kit (Intron Biotechnology, Sungnam, Korea) supplemented with half of a protein inhibitor cocktail tablet (Roche, Penzberg, Germany), after which it was centrifuged at 13,000 rpm for 5 min. The prepared proteins were then electrophoresed through a 10% sodium dodecyl sulfate-polyacrylamide gel electrophoresis (SDS-PAGE) gel, after which they were transferred onto a nitrocellulose membrane (Amersham Biosciences, Corston, UK) for 2 h at 40 V in transfer buffer (25 mM Trizma-base, 192 mM glycine, and 20% methanol). The efficiency of the transfer and equal protein loading were determined by staining the membrane with Ponceau, while the gel was stained with Coomassie blue (both from Sigma-Aldrich Co.). Appropriate dilutions of primary antibodies, rabbit polyclonal antibodies against anti-vascular endothelial growth

factor (VEGF) (1:3,000, 500-P131; PeproTech, Rocky Hill, NJ, USA), anti-collagen (1:1,000, ab292; Abcam, Cambridge, UK), anti-JNK (1:1,000, #9252), anti-phospho-c-Jun N-terminal kinase (JNK; 1:1,000, #9251), anti-p38 (1:1,000, #9212), anti-phospho-p38 (1:1,000, #9211), anti-phospho-extracellular signal-regulated kinase (ERK; 1:1,000, #9101) anti-Smad2/3 (1:1,000, #5678) (all from Cell Signaling Technology, Danvers, MA, USA), anti-ERK (1:1,000, sc-94; Santa Cruz Biotechnology, Inc., Santa Cruz, CA, USA), rabbit monoclonal antibodies against anti-phospho-Smad2/3 (1:1,000, #8828; Cell Signaling Technology) and mouse monoclonal antibodies against β-actin (1:3,000, A5316; Sigma-Aldrich Co.) were added to the membranes and allowed to hybridize overnight at 4˚C. After the antibodies were removed, the membrane was washed 3 times in solution composed of 10 mM Trizma-base (pH 7.6), 150 mM NaCl, and 0.05% Tween-20 for 10 min. The primary antibody-conjugated membranes were then incubated with horseradish peroxidase-conjugated anti-secondary antibody for 1 h at room temperature. The membrane was then washed again as described above and developed using an enhanced chemiluminescence detection system (Amersham Bioscience). Finally, the results were quantified using the Image Analyzer System (Eastman Kodak 2000MM; Eastman Kodak, Rochester, NY, USA) and expressed as the fold increase over the control values. All results were confirmed by two independent researchers conducting the experiments at least twice.

Enzyme-linked immunosorbent assay (ELISA) for transforming growth factor (TGF)-β1. The concentrations of total TGF-β1 in serum were measured using the Legend Max Total TGF-β1 ELISA kit (BioLegend, San Diego, CA, USA) according to the manufacturer's instructions. Briefly, the capture antibody-coated wells in Nunc C bottom immunoplates supplied in the kit were washed 3 times with washing solution. The serum samples and standards were then added to the wells, after which the plates were incubated at room temperature for 2 h. After washing 3 times, TGF-β1 detection antibody solution was added to each well followed by incubation at room temperature for 1 h with shaking. The wells were then washed with washing solution, after which HRP-conjugated detection antibodies were diluted 5,000-fold with conjugate diluent (50 mM Tris, 0.14 M NaCl, 1% BSA, 0.05% Tween-20, pH 8.0) and transferred to each well. The plates were subsequently incubated at room temperature for 30 min, then washed 3 times with washing solution. An enzyme reaction was initiated by adding substrate solution and incubating the plate at room temperature in the dark for 30 min. Finally, the reaction was terminated by adding a stop solution, and the absorbance at 450 nm was measured within 30 min using a microplate reader (Molecular Device, Sunnyvale, CA, USA).

Statistical analysis. One-way ANOVA (SPSS for Windows, Release 10.10, Standard Version; SPSS, Inc., Chicago, IL, USA) was used to identify significant differences between the GZ and the three SCT-CM-treated groups. In addition, differences in the responses of the SCT-CM- and other two SCT-CM-treated groups (FSCT-CM and ASCT-CM) were evaluated using a post-hoc test (SPSS for Windows, release 10.10, standard version; SPSS, Inc.) of the variance and significance. All values are reported as the means ± SD, and a P-value <0.05 was considered to indicate a statistically significant difference.

Results

Physical properties of the three SCT-CMs. The surface and fracture surface morphology of the three SCT-CMs was observed by SEM. Two distinct type structures were detected on the fracture surface the three SCT-CMs. The first structure consisted of randomly arranged fibrils with a variety of empty spaces present in the internal matrix of both the SCT-CM and FSCT-CM, although some differences in the ultrawave structures were observed between both CMs. The gap length of the interlayer on the fracture surface was greater (75%) in the FSCT-CM compared with the SCT-CM (Fig. 1A, B and D). The second type, which consisted of a large number of small pores distributed in the same area, was only observed with the ASCT-CM. The average pore diameter of the ASCT-CM was 1.67 μm (Fig. 1C and D). However, no specific differences or unique features were observed upon surface morphological analysis (Fig. 1A-C, inset on the top left corner of the image). Therefore, these results suggest that the FSCT-CM had a highly interlayered structure and a variety of empty spaces that could respond to high water absorbance and capacity.

The tensile strength of the FSCT-CM (1.64±0.51 N/mm^2) was approximately 993 and 115% greater than that of the SCT-CM (0.15±0.01 N/mm^2) and ASCT-CM (0.76±0.06 N/mm^2), although the level of elongation was only higher in the ASCT-CM (94.17±12.67%) compared with the SCT-CM (31.14±4.37%) and FSCT-CM (28.59±2.28%) (Fig. 2A and B). Moreover, in the analysis for moisture regulatory ability, the three SCT-CMs exhibited different properties as regards the fluid uptake rate and WVTR. The fluid uptake rate of the FSCT-CM was maintained at a constant level (approximately 120%), whereas that of the SCT-CM remained at a very low level. However, the fluid uptake rate of the ASCT-CM rapidly increased to 210% within 8 h and was maintained at a constant level (Fig. 2C). In addition, the WVTR of the three SCT-CMs exhibited a similar pattern during the experimental period, although that of the FSCT-CM was maintained at a lower level than the other two CMs. Until the time point of 24 h, the WVTR of the three CMs was rapidly enhanced; however, these levels slowly decreased to 102 (SCT-CM), 83 (ASCT-CM) and 69 g/m^2/h (FSCT-CM) within 72 h (Fig. 2D). Taken together, the above-mentioned results provide evidence that the FSCT-CM has good physical properties and may thus be used as a dressing for surgical wounds on the skins of mammals.

Effect of the three SCT-CMs on the wound healing process. To determine how stimulation with the three SCT-CMs affects the healing process of the wounded skin, the closing rate of a round area 8 mm in diameter and 2-4 mm in depth was measured for skin covered with one of the three SCT-CMs for 14 days. We noted that the most significant changes in the wound area occurred during days 3-6 and 12-14. In the FSCT-CM sample, the relative area of the wound decreased to 0.3±0.06 from 1.0±0.08 at 14 days, while only a 0.77±0.01 change in the same sample was observed during the first 6 days. Similar results were also observed in the SCT-CM-treated group, although the decrease rate varied in both groups. In other words, the wound closing rate was 12.5-37.5% greater in the FSCT-CM and SCT-CM sample than in the GZ sample during the first 3-6 days. The closing rate of the FSCT-CM sample remained the fastest

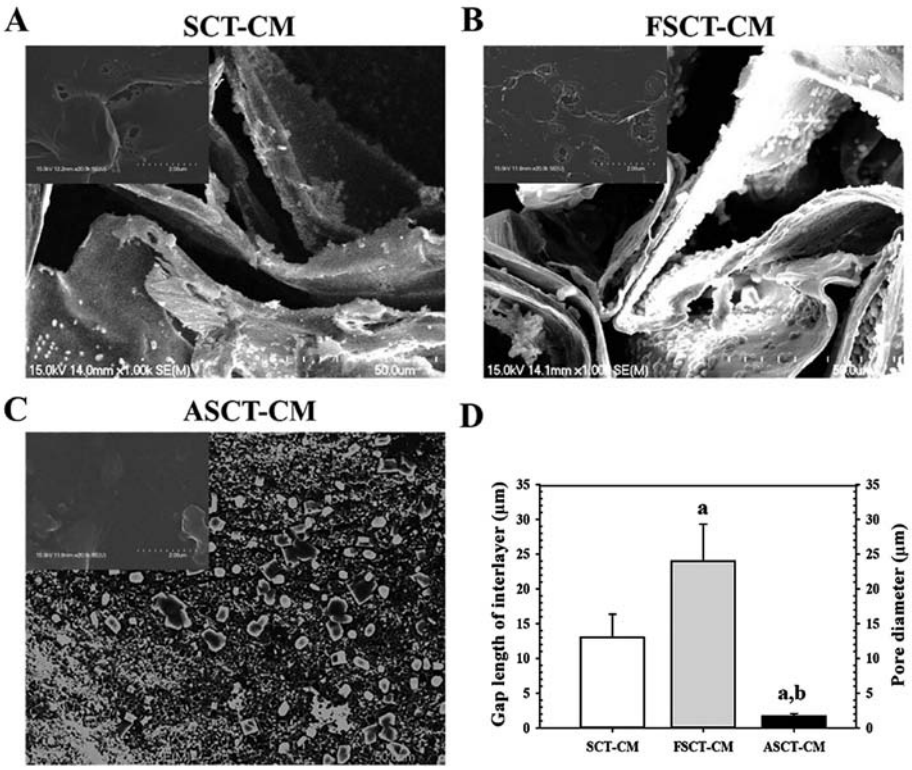

Figure 1. Scanning electron microscopy (SEM) images of the three *Styela clava* tunic-cellulose membranes (SCT-CMs). The ultrastructure of the fracture surface of (A) SCT-CM, (B) FSCT-CM and (C) ASCT-CM was observed by SEM at x1,000 magnification as described in the Materials and methods. The images in upper left corner represent the ultrastructure of the surface. (D) The gap length of interlayer in SCT-CM and FSCT-CM and pore size (μm) of each ASCT-CM was measured was measured using Leica Application Suite as described in the Materials and methods. Three to five films per group were assayed in duplicate by SEM. [a]P<0.05 compared to SCT-CM; [b]P<0.05 compared to FSCT-CM. FSCT-CM, freeze-dried SCT-CM; ASCT-CM, sodium alginate-supplemented SCT-CM.

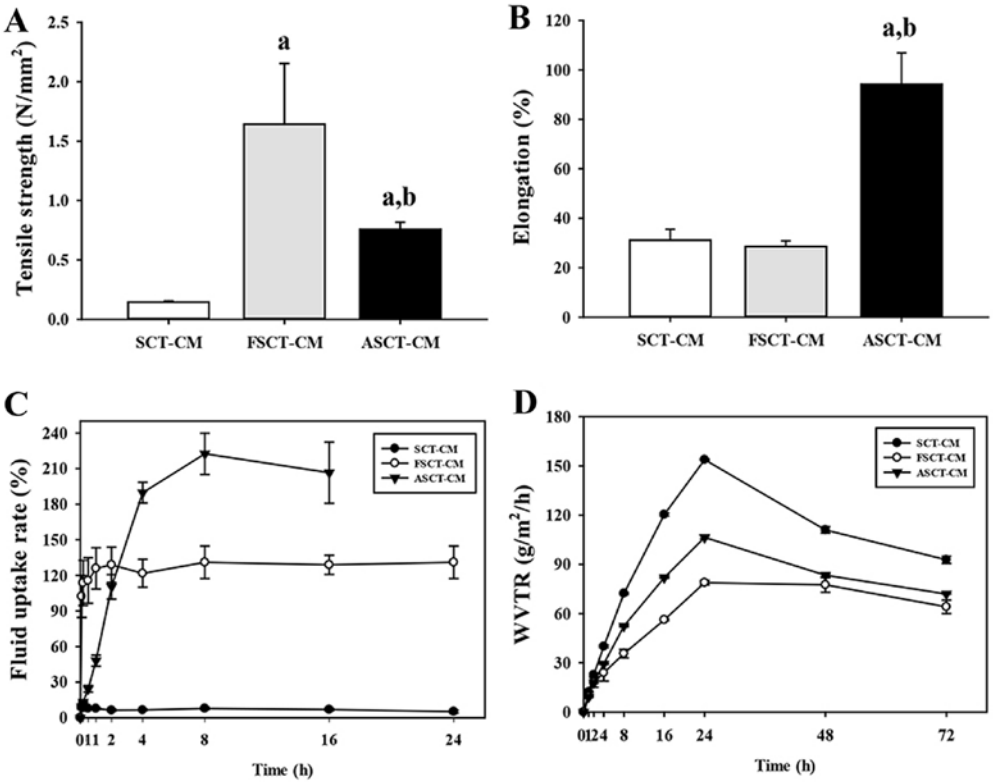

Figure 2. Physical properties of the three *Styela clava* tunic-cellulose membranes (SCT-CMs). Physical properties including (A) Tensile strength, (B) elongation, (C) fluid uptake rate and (D) water vapor transmission rate (WVTR), which were analyzed using three to five films per group were assayed in duplicate by 4 analyses. [a]P<0.05 compared to SCT-CM; [b]P<0.05 compared to FSCT-CM. FSCT-CM, freeze-dried SCT-CM; ASCT-CM, sodium alginate-supplemented SCT-CM.

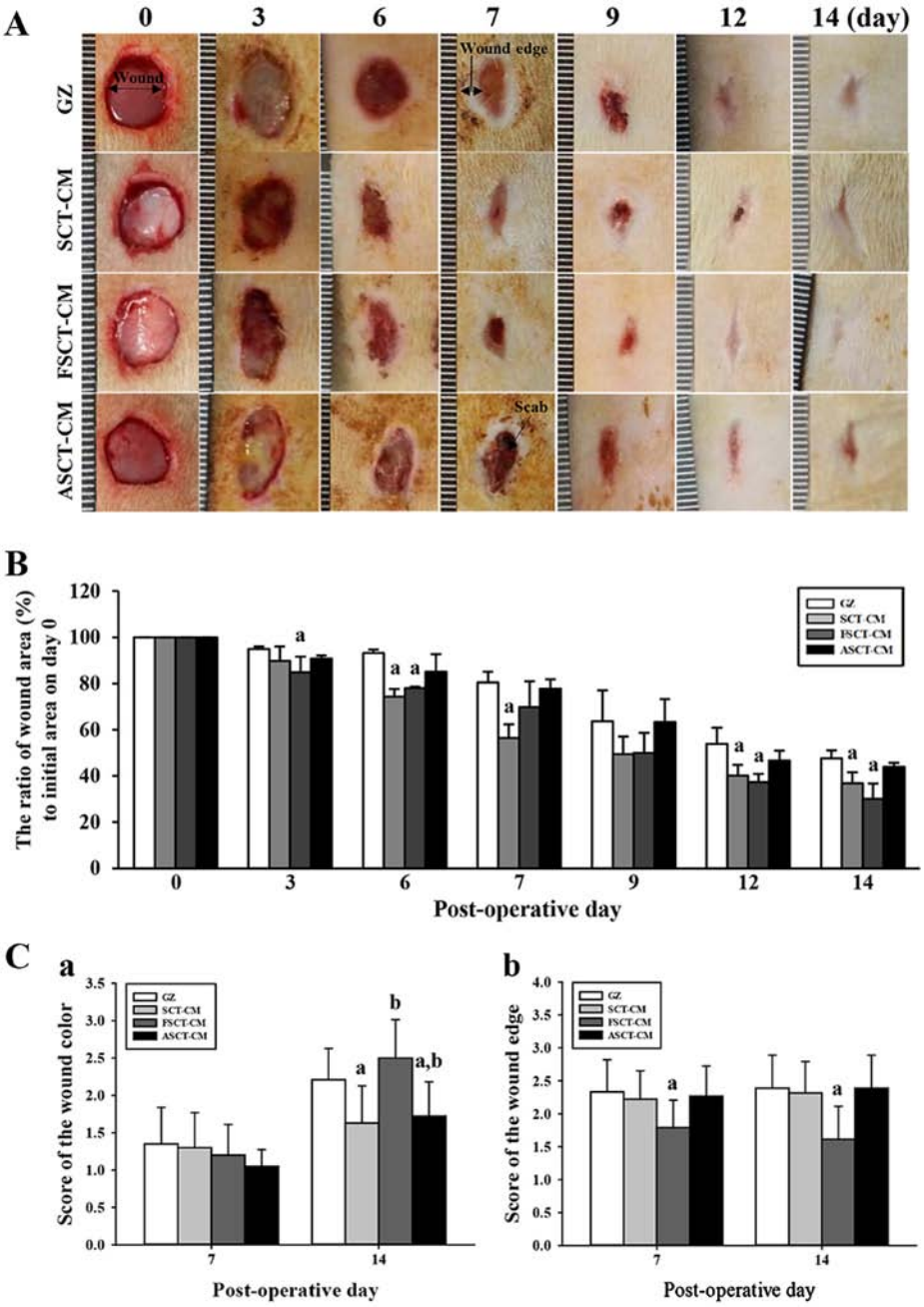

Figure 3. Healing pattern of wound skin with time. At each time point, images of the surgically wounded skin of the rats of each group were taken, and the morphological features were evaluated. (A) Macro-observation of experimental wound healing at various times post-surgery. (B) The ratio of wound area (%) to initial area on day 1 was measured with time. The wound size was measured in triplicate in each test. (C) The total score for wound color (1, red; 2, pink; 3, pale; 4, cyan) and edge (1, without granulation tissue; 2, little granulation tissue; 3, very granulation tissue) were defined as the sum of the individual scores. Five or six wounds were assayed in triplicate using wound area analysis. Date are reported as the means ± SD. $^{a}P<0.05$ relative to the gauze (GZ)-treated group. FSCT-CM, freeze-dried SCT-CM; ASCT-CM, sodium alginate-supplemented SCT-CM.

among the samples until the final observation after 14 days, at which point the wound skin was completely repaired in all the treatment groups (Fig. 3A and B). However, the ASCT-CM-treated group did not exhibit any significant alterations when compared with the GZ-treated group. Additionally, the wound color score was significantly higher in all the treatment groups at 14 days than at 7 days. Among these groups, the highest level was detected in the FSCT-CM-treated group (Fig. 3C-a). Furthermore, the score of the wound edge only decreased in the FSCT-CM-treated group compared with the GZ-treated group, although the SCT-CM- and ASCT-CM-treated groups maintained a constant level (Fig. 3C-b). Taken together, these results suggest that the enhanced ability of the skin to heal the wound and regenerate tissue could be reasonably attributed to the FSCT-CM.

Effect of the three SCT-CMs on tissue regeneration in the wounded skin. The alteration was determined based on the recovery of the epidermis, dermis and hyperdermis of the skin tissue of the rats over the designated period of time (i.e., 7 and

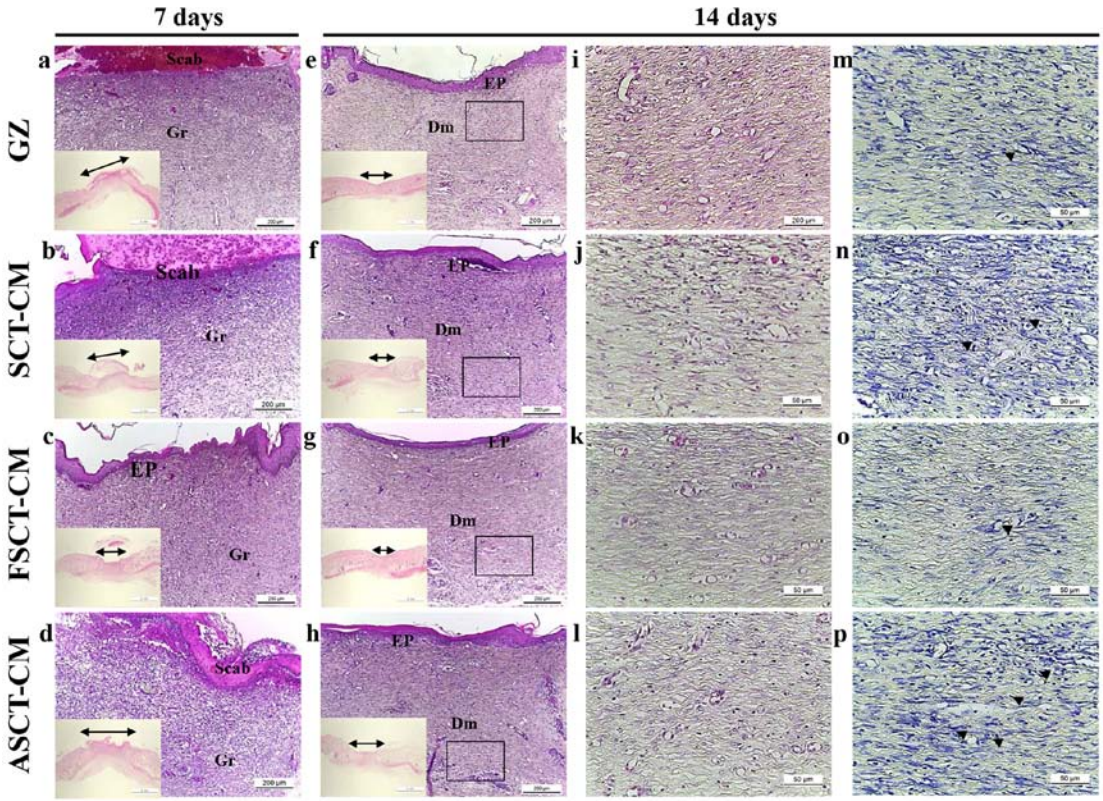

Figure 4. Histologic analyses after *Styela clava* tunic-cellulose membranes (SCT-CMs) application. Hematoxylin and eosin (H&E) stained sections of subcutaneous tissue surrounding the three SCT-CMs applied to SD rats at different time points were observed using a light microscope at magnifications of x40 (a-h), including x10 in the corner of each image and x400 (i-l). In addition, the infiltration of mast cells in the slide sections of skin tissue were detected by toluidine blue staining followed by observation at x400 magnification (m-p). The arrow heads indicate infiltrated mast cells in the dermis of the skin. The double-headed arrows indicate a length of re-epithelization in the epidermis of the skin. FSCT-CM, freeze-dried SCT-CM; ASCT-CM, sodium alginate-supplemented SCT-CM; GZ, gauze.

14 days). To examine the therapeutic effects of the three SCT-CMs on the histological structure of surgical wounds on the skin, the thickness of the epidermis and dermis, as well as the number of blood vessels and mast cells were monitored in the GZ-, SCT-CM-, FSCT-CM- and ASCT-CM-treated rats. After the first 7 days post-surgery, the thickness of the total epidermis was significantly enhanced by approximately 35.9% in the FSCT-CM-treated group compared with the GZ-treated group, while it was maintained at a constant level in the SCT-CM- and ASCT-CM-treated groups. At 14 days post-surgery, both the FSCT-CM- and SCT-CM-treated groups had a thinner epidermis than the GZ-treated group, although a larger decrease was detected in the FSCT-CM-treated group; nevertheless, the rate of change was reflected in the stratum basal and stratum granulosum (Fig. 4 and Table I). In addition, the inflammatory reaction was measured by counting the immune cells in the dermis region. A significant decrease in the number of immune cells was detected in the FSCT-CM-treated group compared with the GZ-treated group, while a constant level was maintained in the other groups. Furthermore, a similar pattern in the number of mast cells was also observed. Only the FSCT-CM-treated group exhibited a decrease of approximately 41.0% in the number of mast cells at 7 days post-surgery, while a decrease of 48.4% was measured at 14 days post-surgery (Table I). Taken together, these results suggest that the use of the FSCT-CM enhanced tissue regeneration, including increasing epidermal thickness, promoting the formation of blood vessels, and suppressing the inflammatory response in the skin tissue of SD rats.

Effect of the three SCT-CMs on angiogenesis in the wounded skin. To evaluate the effects of the three SCT-CMs on angiogenesis in the dermis of wounded skin, we measured the number of blood vessels and the expression level of VEGF in a subset of groups for different times. The number of blood vessels in the dermis was only higher in the FSCT-CM-treated group compared with the GZ-treated group at 7 days post-surgery, while the levels remained constant in the SCT-CM- and ASCT-CM-treated groups. However, the level rapidly decreased in at 14 days post-surgery (Fig. 5A). In addition, the expression of VEGF, an important signaling protein involved in both vasculogenesis and angiogenesis, was similar to the number of blood vessels at 7 and 14 days post-surgery. A high level of VEGF expression was measured at day 7 post-surgery in the FSCT-CM-treated group, although a constant level was maintained in the other groups. However, this level markedly decreased in the same group at 14 days post-surgery (Fig. 5B). Therefore, the results of the present study indicate that the use of the FSCT-CM stimulates angiogenesis by enhancing the expression of VEGF.

Effect of the three SCT-CMs on the formation of connective tissue in wounded skin. To evaluate the effects of treatment with the three SCT-CMs on the formation of connective tissue

Table I. Alterations of the histopathological properties of wounded skin treated with SCT-CMs.

		Histopathological analysis			
Items	Day	GZ	SCT-CM	FSCT-CM	ASCT-CM
Epidermis					
Thickness of total	7	23.14±2.44	24.85±1.92	31.44±3.13[a]	21.89±2.63
epidermis (μm)	14	67.52±3.9	64.34±4.95	32.53±3.34[a]	61.92±3.41
Thickness of stratum	7	NID	NID	NID	NID
basal (SB) (μm)	14	29.49±3.65	26.28±3.63	13.91±3.74[a]	25.07±3.27
Thickness of stratum	7	NID	NID	NID	NID
spinosum (SS) (μm)	14	30.29±1.91	29.07±2.67	11.07±2.82[a]	23.8±2.98[a]
Thickness of stratum	7	NID	NID	NID	NID
granulosum (SG) (μm)	14	8.47±1.31	4.59±0.35a	8.68±0.69	5.02±0.93[a]
Thickness of	7	1656.75±94.97	1002.92±13.01[a]	1515.08±18.74[a]	1813.49±37.48[a]
dermis (μm)	14	1365±56.69	1450.75±23.34[a]	1246.75±32.92[a]	1544.25±41.25[a]
No. immune cells	7	41.67±3.79	43.67±3.21	34.67±4.51	41±2
(cells/0.16 mm^2)	14	25.33±2.52	30±5.57	15.33±3.5[a]	24.67±1.53
No. mast cells	7	57.67±2.52	52.33±9.87	34±6.08[a]	66.33±7.37
(cells/0.01 mm^2)	14	22.75±3.77	31.75±3.3[a]	11.75±2.99[a]	29±5.83

Data represent the means ± SD from 3 replicates. [a]P<0.05 compared to the GZ-treated group. NID, not identified; SCT-CM, *Styela clava* tunic-cellulose membranes; FSCT-CM, freeze-dried SCT-CM; ASCT-CM, sodium alginate-supplemented SCT-CM; GZ, gauze.

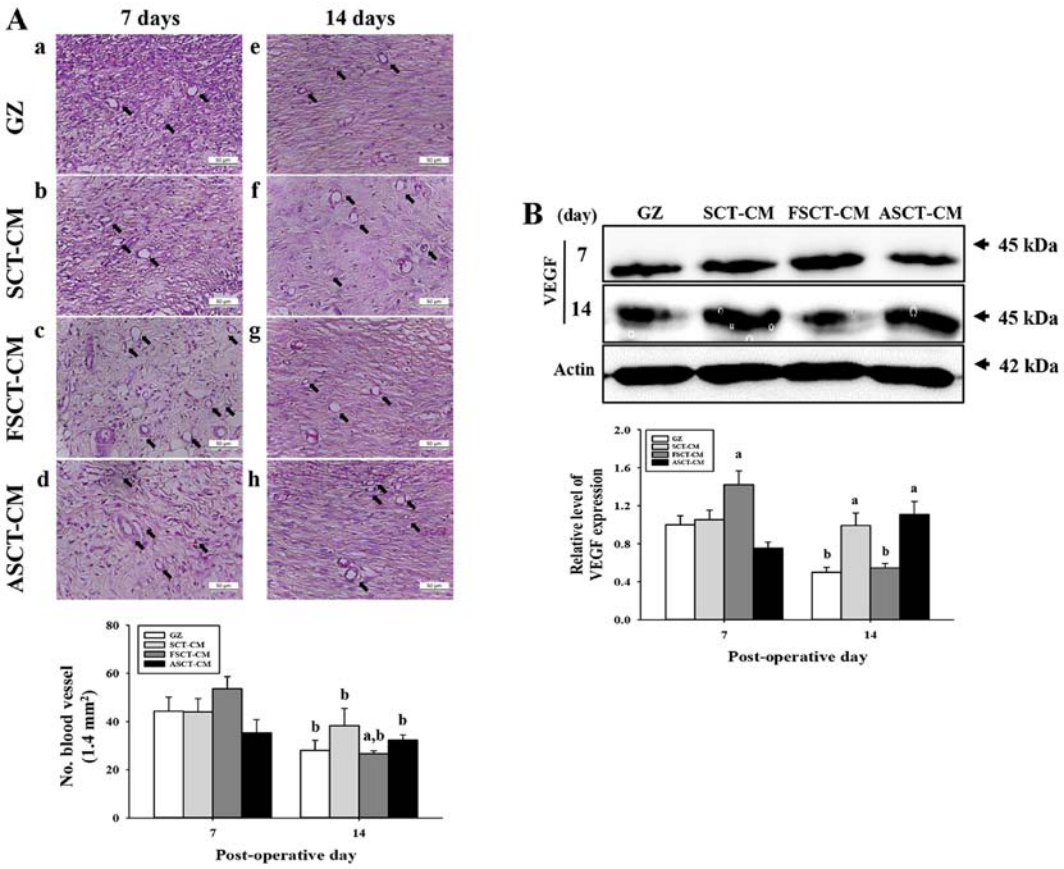

Figure 5. Analysis for angiogenesis. (A) The number of blood vessels in hematoxylin and eosin (H&E)-stained sections of subcutaneous tissue surrounding the three *Styela clava* tunic-cellulose membranes (SCT-CMs) applied to SD rats at different time points was measured using Leica Application Suite as described in the Materials and methods. The arrows indicate the newly formed blood vessels in the subcutaneous tissue. (B) Western blot analysis of VEGF in the homogenate mixture prepared from the wound skin was detected using the specific primary antibody. The value was defined as 1 [gauze (GZ)-treated group] for the acquisition of other relative values. Data represent the means ± SD from 3 replicates. [a]P<0.05 compared to the GZ-treated group; [b]P<0.05 compared to the level in same group on day 7. FSCT-CM, freeze-dried SCT-CM; ASCT-CM, sodium alginate-supplemented SCT-CM.

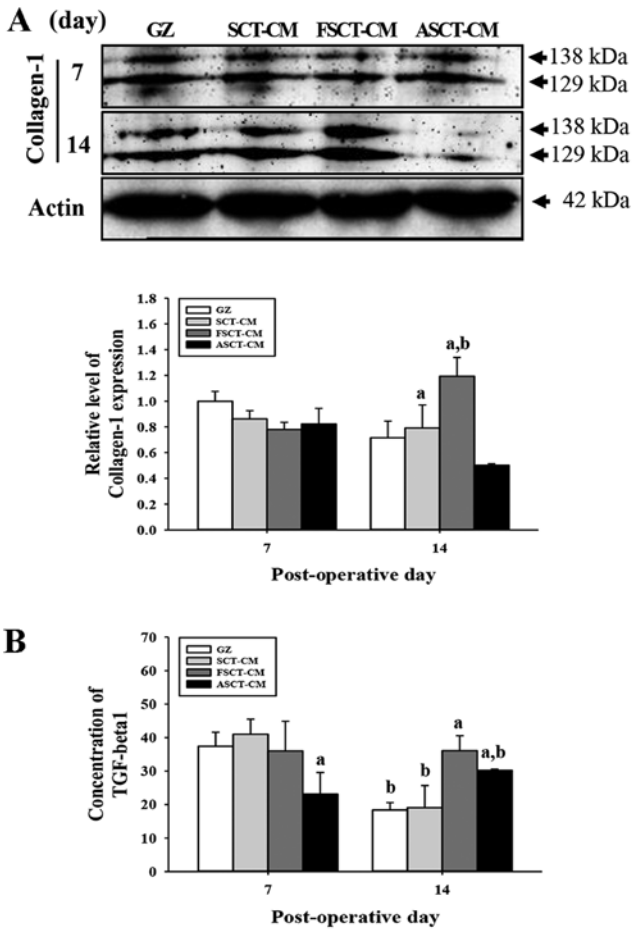

Figure 6. Analysis of collagen-1 expression and tumor growth factor (TGF)-β1 concentration. (A) Western blot analysis of collagen-1 in the homogenate mixture prepared from the wound skin was detected using the specific primary antibody. The value was defined as 1 [gauze (GZ)-treated group] for the acquisition of other relative values. (B) Concentration of TGF-1β in the blood serum. The ELISA kit used in this experiment can detect TGF-1β at 7.8 to 500 pg/ml. Data represent the means ± SD of 3 replicates. [a]P<0.05 compared to the GZ-treated group; [b]P<0.05 compared to the level in the same group on day 7. FSCT-CM, freeze-dried SCT-CM; ASCT-CM, sodium alginate-supplemented SCT-CM.

in the wounded skin, we measured the expression level of collagen and the concentration of TGF-β1 in a subset of groups at different times. At 7 days post-surgery, there was no significant alteration in the expression of collagen-1 in any of the group subsets. However, these levels were rapidly increased in the FSCT-CM-treated group at 14 days, while they decreased in the ASCT-CM-treated group (Fig. 6A). Furthermore, to determine whether the overexpression of collagen was accompanied by an increase in the concentration of TGF-β1, the the TGF-β1 concentrations in the serum of the rats in the group subsets were compared. Overall, the concentration of TGF-β1 was very similar to the expression of collagen-1, although the level in the ASCT-CM-treated group differed slightly. At 7 days post-surgery, a significant decrease in the TGF-β1 concentration was detected in the ASCT-CM-treated group, whereas the level remained constant in the other groups. At 14 days post-surgery, the level increased significantly in the FSCT-CM- and ASCT-CM-treated groups compared with the GZ-treated group (Fig. 6B). Overall, these findings indicate that the use of the FSCT-CM induced an increase in collagen levels via the regulation of TGF-β1 concentration during the later stages of the wound skin repair process.

Molecular mechanisms underlying skin re-epithelialization and wound repair with the use of the three SCT-CMs. Re-epithelialization of wounded skin is accompanied by the secretion of epidermal growth factors (EGFs), fibroblast growth factor (FGF) family members, TGF-β, and some chemokines, which stimulate fibroblasts and increase the expression of smooth muscle actin in response to wound contraction and collagen synthesis (19). Among these, the TGF-β1 signaling pathway includes Smad2/3 in the Smad-dependent pathway and the MAP kinase protein in the Smad-independent pathway (20,21). To investigate the molecular mechanisms of re-epithelialization in wounded skin occurring after the use of the three SCT-CMs, changes in the regulatory factors of the TGF-β1 signaling pathway consisting of the Smad-dependent and -independent pathway were measured by western blot analysis in the group subsets. In the case of the Smad-dependent pathway, the expression of p-Smad2/3 at 7 days post-surgery was higher in the FSCT-CM-treated group than in the GZ-, SCT-CM- and ASCT-CM-treated groups. However, a different pattern was observed at 14 days post-surgery. The expression of p-Smad2 was lower in the SCT-CM-treated groups than in the GZ-treated group, although the lowest level was observed in the ASCT-CM treated group. However, the expression of p-Smad3 was higher in the SCT-CM-treated groups than in the GZ-treated group (Fig. 7). In the case of the Smad-dependent pathway, alterations in the phosphorylation of downstream regulators in the MAP kinase pathway were also detected in the three SCT-CM-treated groups. The expression level of p-JNK and p-p38 reflected the expression level of p-Smad2 and p-Smad3 well. The highest level of both proteins was detected in the FSCT-CM-treated group at 7 days post-surgery. However, at 14 days post-surgery, a high level of p-JNK and p-p38 was detected in the three SCT-CM-treated groups compared with the GZ-treated group, although the highest level was observed in the ASCT-CM-treated group. Moreover, the FSCT-CM-treated group exhibited a higher level of p-ERK than the other groups at 14 days post-surgery (Fig. 7B-e). Therefore, these results suggest that the use of the FSCT-CM may significantly accelerate angiogenesis through the stimulation of the TGF-β1 signaling pathway during the early stages of wound healing.

Toxicity of the three SCT-CMs. To investigate the toxicity of the three SCT-CMs toward the livers and kidneys of the SD rats, alterations in body weight, metabolic enzymes and histopathology were investigated in blood serum and liver and kidney tissue using serum biochemical analysis and histological analysis. No significant alterations in body weight over 14 days were detected in any of the three SCT-CM-treated groups when compared with the GZ-treated group (Table II). Liver toxicity analysis revealed no increase in the levels of the three liver toxicity indicators, specifically ALP, AST and ALT, between the three SCT-CM-treated groups and the GZ-treated group at either time point, although significantly higher levels of AST and ALT were detected in the ASCT-CM-treated group on day 7 (Table III). The results of kidney toxicity analysis were similar to those observed in the liver toxicity analysis. Specifically, the BUN and CRE levels in serum did not increase

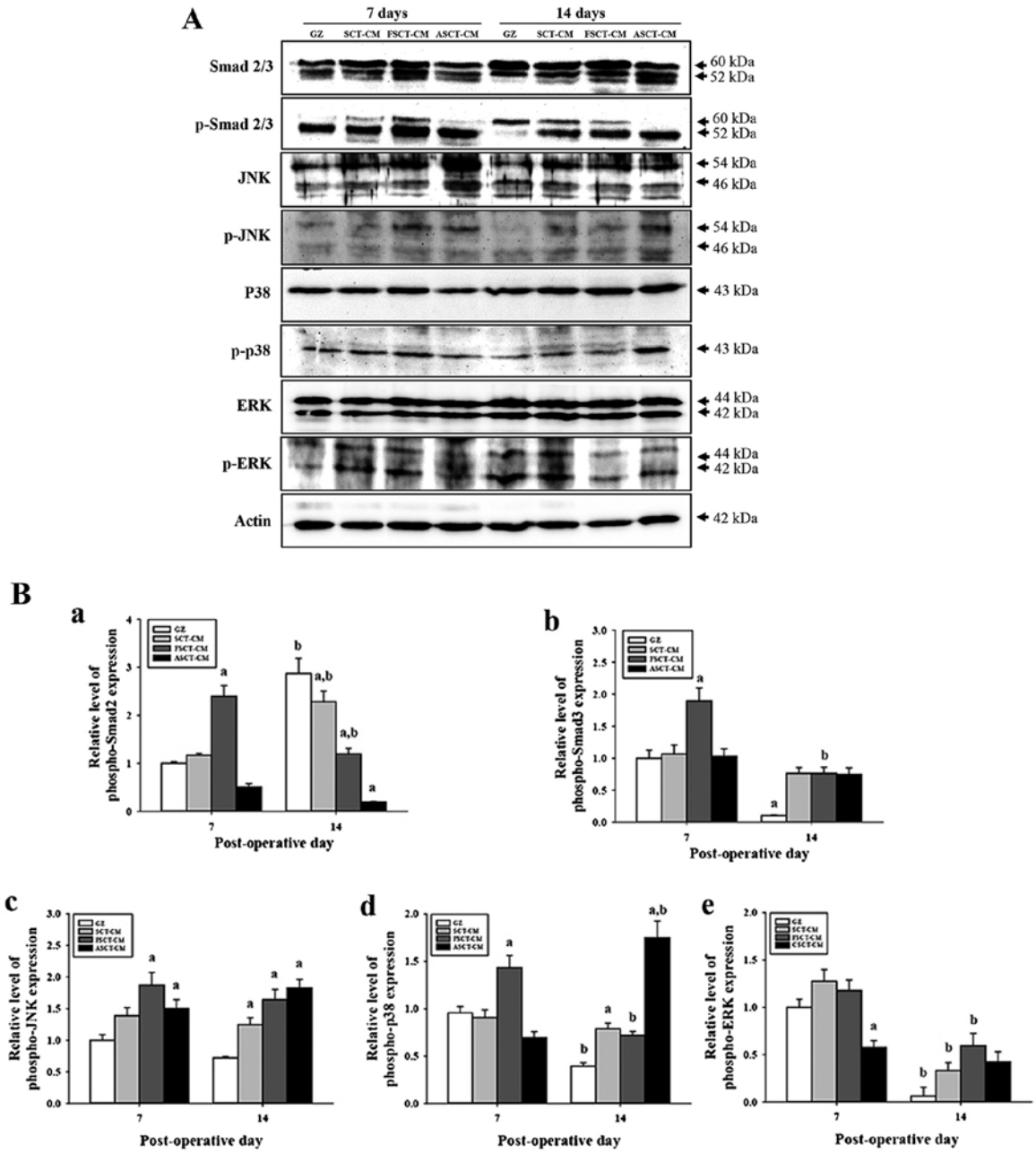

Figure 7. Analysis of the downstream signaling pathway of tumor growth factor (TGF)-β1. (A and B) Western blot analysis of Smad2/3, JNK, p38, ERK and β-actin in the homogenate mixture prepared from the wounded skin was detected using specific primary antibodies. The value was defined as 1 [gauze (GZ)=treated group] for the acquisition of other relative values. Data represent the means ± SD from 3 replicates. [a]P<0.05 compared to the GZ-treated group; [b]P<0.05 compared to the level of the same group on 7 days. FSCT-CM, freeze-dried SCT-CM; ASCT-CM, sodium alginate-supplemented SCT-CM.

Table II. Alterations in body weight of the SD rats following the application of the SCT-CMs.

Day	GZ	SCT-CM	FSCT-CM	ASCT-CM
0	259.3±12.37	262.9±15.07	262.6±13.07	267.8±10.05
3	267.5±16.32	270.2±13.21	260.3±13.4	270.5±13.89
6	282.3±17.84	288.5±11.34	267.9±14.11	284.6±14.59
9	295±33.85	311.6±21.73	291±15.62	298.4±10.33
12	310.8±29.43	324.6±23.29	301±18.08	308±14.2

Data represent the means ± SD from 3 replicates. SCT-CM, *Styela clava* tunic-cellulose membranes; FSCT-CM, freeze-dried SCT-CM; ASCT-CM, sodium alginate-supplemented SCT-CM; GZ, gauze.

significantly in the three SCT-CM-treated groups, regardless of the exposure time (Table III). To investigate histological alterations, liver and kidney sections were stained with H&E and observed microscopically. No significant pathological changes were detected between the liver and kidney tissue of the rats in any of the groups (Fig. 8), suggesting that the use of the three SCT-CMs for a short period of time did not induce toxicity to the livers and kidneys of the SD rats.

Discussion

Cellulose and its derivatives have been applied as drug coating materials, blood coagulants, artificial kidney membranes,

Table III. Alterations in the serum levels of the biochemical markers, ALP, AST, ALT, BUN and CRE.

Day	Items	GZ	SCT-CM	FSCT-CM	ASCT-CM
7	ALP	333±91.92	365.33±17.95	357±55.58	337.33±57.84
	AST	93±2.83	98.67±8.5	87.67±12.42	125.5±37.48[a]
	ALT	49±1.41	61.67±5.13	55±15.72	79±14.14[a]
	BUN	18.73±3.84	20.17±2.66	17.95±1.75	20.48±1.85
	CRE	0.7±0.01	0.68±0.06	0.68±0.03	0.59±0.1
14	ALP	328±43.26	361.4±86.71	1403.4±132.94[a]	380.25±66.09
	AST	86.8±10.21	77.4±7.99	83.33±15.53	98.75±27
	ALT	49.4±5.55	51.6±10.14	60.2±19.5	62.5±13.48
	BUN	20.14±2.12	20.64±1.54	21.04±2.06	20.78±1.81
	CRE	0.66±0.05	0.63±0.03	0.61±0.04	0.6±0.06

Data represent the means ± SD from 3 replicates. [a]P<0.05 compared to the GZ-treated group; [b]P<0 compared to the level in the same group on day 7. SCT-CM, *Styela clava* tunic-cellulose membranes; FSCT-CM, freeze-dried SCT-CM; ASCT-CM, sodium alginate-supplemented SCT-CM; GZ, gauze; ALP, alkaline phosphatase; AST, aspartate aminotransferase; ALT, alanine aminotransferase; BUN, blood urea nitrogen; CRE, creatinine.

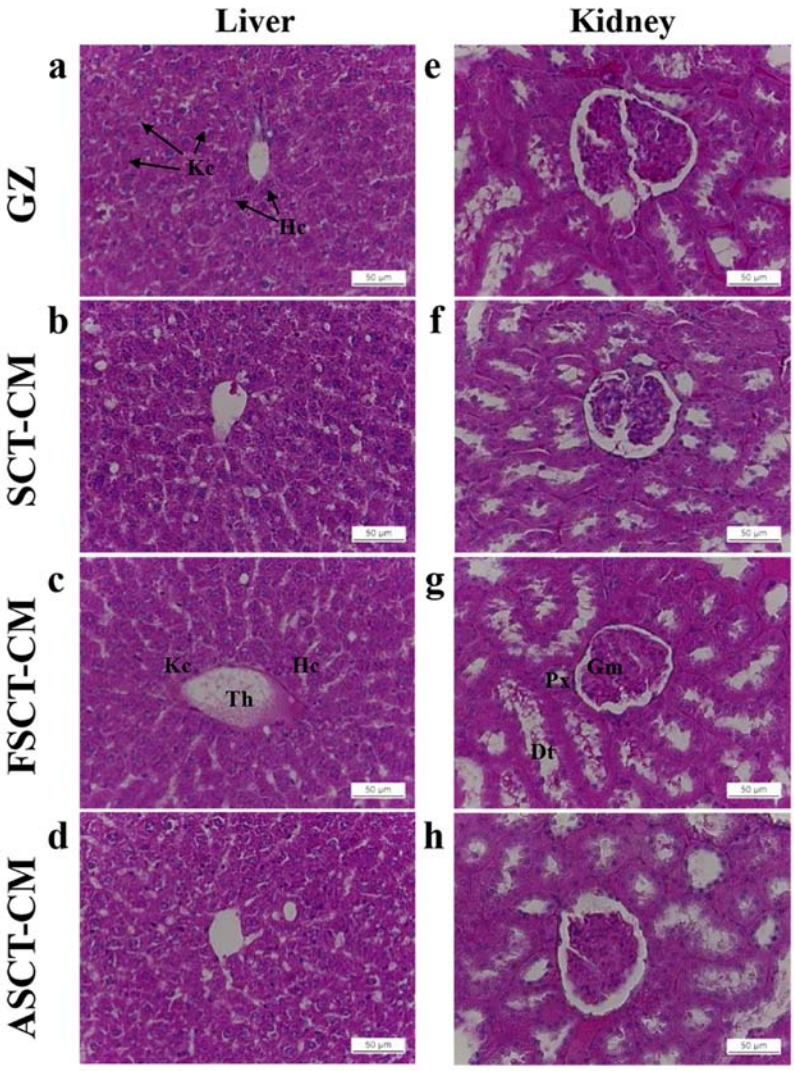

Figure 8. Toxicity analysis of *Styela clava* tunic-cellulose membranes (SCT-CMs) application. Liver and kidney tissue of SD rats was prepared on a histological slide, and cellular morphology was viewed at x400 magnification. Data represent the means ± SD from 3 replicates. [a]P<0.05 compared to the gauze (GZ)-treated group; [b]P<0 compared to the level in the same group on day 7. FSCT-CM, freeze-dried SCT-CM; ASCT-CM, sodium alginate-supplemented SCT-CM. Kc, kupfer cell; Hc, hepatocyte; Th, terminal hepatic vein; Gm, glomeruli; Px, proximal convoluted tubules; Dt, distal convoluted tubules.

antitumor drugs, blood-compatible materials and supports for immobilized enzymes in various medical fields (22,23). CM has recently received a great deal of attention as a novel biomedical material for the treatment of various wounds as it does not require special treatment for the elimination of risk factors, such as immune response and viral risk following chitosan treatment (24,25). Therefore, in this study, we attempted to obtain additional evidence of the potential for SCT-CM medical applications and then investigated the therapeutic effects and toxicity of the three SCT-CMs in surgical wounds of rat back skin. The results of the present study clearly demonstrated that the FSCT-CM promoted the improvement of wound skin symptoms, re-epithelization, granulation tissue formation and angiogenesis without exerting any toxic effects.

In wound dressing, the porous, sponge and multilayer structure provide several benefits, including absorbing large amount of exudate, increasing the efficiency of drug release, good contacting ability and strong adhesion to the wound surface (26). In this study, two different types of structures on the fracture surface were observed in the SEM image of the three SCT-CMs. The multilayer structure on the fracture surface of the SCT-CM and FSCT-CM was very similar with that of the SCT-CF20-F prepared with 3% SCT in [Amim]Cl in a previous study (26). However, the porous structures detected in the ASCT-CM (1.67 μm in diameter) were observed in many regenerated cellulose films and membranes although their pore size was varied in each one. Regenerated cellulose film prepared by coagulating with sulfuric acid displayed a porous structure calculated to be 186 and 80 nm in diameter on the free surface and fracture surface (27). In addition, regenerated cellulose hydrogel films presented a fibrous internetwork and porous structure with diameter of approximatel 20 nm (28).

The enhanced physical properties, including tensile strength and elongation are required to satisfy the requirements of a wound dressing. In a previous study, the tensile strength of the regenerated cellulose film with plasticizers prepared with 5% cellulose in [Amim]Cl was increased to 70-80 Mpa although elongation was approximately 6% (29). However, in this study, the three SCT-CMs prepared in similar conditions with those of the previous study exhibited an increased level of tensile strength and elongation. In particular, the FSCT-CM exhibited the highest strength and lowest elongation level among the three SCT-CMs. These differences in the value of tensile strength and elongation could be caused by adding platicizer.

WVTR among various physical properties of wound dressing tightly correlated with the speed and time required for wound repair in the skin tissue. The excessively high level of WVTR value stimulates the scare formation in the wound area as the wound can dry rapidly. However, the wound repair process can be impeded by accumulating exudates, resulting in an enhanced risk of bacterial infection when the WVTR level is too low (30). Generally, the WVTR value was measured as 8.5 g/m^2/h in the normal skin although this value was approximately 11.6 g/m^2/h in the injured skin (31). In this study, the FSCT-CM exhibited a stable value on the fluid uptake rate and WVTR compared with the SCT-CM and ASCT-CM. The WVTR value of the FSCT-CM gradually increased to approximately 72 g/m^2/h within 24 h and then maintained this level from 24 to 72 h. These levels were also higher, being 8.5-fold those of normal skin (8.5 g/m^2/h) (31) and higher, being 3-3.2-fold those of 23-25 g/m^2/h of regenerated cellulose/collagen composite hydrogel films showing good equilibrium-swelling ratio, air permeability and water retention properties (28). However, this level of FSCT-CMs was significantly lower than wound dressings available on the market such as Geliperm (375.39 g/m^2/h; Geistlich Ltd., Wolhusen, Switzerland) and Vigilon (390.01 g/m^2/h; Bard Ltd., West Sussex, UK) (32).

The results presented herein demonstrated that the use of the SCT-CM and FSCT-CM stimulated wound closure in surgically-injured skin of SD rats. The enhancement of the wound closure rate, as well as the regeneration of normal tissue, including a decrease in the wound edge, was strongly detected within 3-6 and 12-14 days of surgical injury (Fig. 4). These results were consistent with the results of several previous studies, showing that the topical application of several cellulose mixtures significantly increased the rate of wound healing over that of vehicle-treated groups in animals and humans. The diameter of the wound area was shown to decrease in hydrocolloid membrane (HCM)-SCT-treated SD rats when compared with the GZ-treated group (11). Moreover, the topical application of ORC/collagen was found to accelerate diabetic wound closure in C57BL/KsJ (db/db) mice and humans with diabetic foot ulcers (12,33). However, several opposing results in the investigations of wound closure have been recently reported. Specifically, the percentage of wound contraction was lower in crystalline CM-treated Wistar rats than the 0.9% sodium chloride-treated group (10). Therefore, we hypothesized that these differences in wound repair may be caused by differences in the manufacturing process or additives, even though cellulose was used as a basic building material.

Another conclusion of this study is that SCT-CM treatment applied to the back skin of SD rats stimulated the regeneration of surgical wound tissue. Similar results have been reported for surgical wounds on SD rats treated with HCM-SCT or ORC. Application of HCM-SCT into surgical wound skin accelerated wound reepithelization, development of young granulation tissues, and decreasing epidermis thickness when compared with that of the GZ treated group (11). The thickness of the epidermis at 14 days was rapidly recovered to a normal level in the FSCT-CM treated group. Therefore, we propose that FSCT-CM treatment for a longer period of time should be investigated to determine if the skin regeneration is complete.

Immune cells and mast cells are known to participate in the three phases of skin wound healing, inflammatory reaction, angiogenesis and extracellular-matrix reabsorption (34). Therefore, the infiltration of these cells into the dermis of wounded skin is considered a key indicator of inflammatory reaction against the wound dressing materials. Surgical wounds treated with ORC have been shown to have a significantly lower number of infiltrated inflammatory cells when compared with the control group at 5 days post-surgery (35). In addition, a decrease in the infiltration of mononuclear cells was measured in skin wounds treated with crystalline CM at days 14, 21 and 26, even though a constant level was maintained until day 7 (10). In the present study, the number of inflammatory cells and mast cells markedly decreased in the FSCT-CM-treated group at days 7 and 14, while a decrease in the number of mast cells was detected in the SCT-CM treated group at day 14. The results for the later stages agree completely with those of

Table IV. Summary of the properties of the three SCT-CMs applied as wound dressings.

Classification	Contents	SCT-CM	FSCT-CM	ASCT-CM
Preparation	Materials	SCT	SCT	SCT with sodium alginate
	Drying conditions	Drying at room temperature for 24 h	Freeze-drying after drying at room temperature for 24 h	Drying at room temperature for 24 h
Physical properties analyses	Morphologic properties	Randomly arranged fibrils	Randomly arranged fibrils	Many small pores
	Mechanical properties			
	Tensile strength	Low	High	Medium
	Elongation	Medium	Low	High
	Fluid uptake rate	Low	Medium	High
	WVTR	Low	Medium	High
Efficacy analyses	Wound closing	Medium	High	Low
	Re-epithelization	Medium	High	Low
	Angiogenesis	Low	High	Low
	Inflammation	Medium	Low	High
	Connective tissue regeneration	Medium	High	Low
Toxicity analyses	Hephatotoxicity	None	None	None
	Nephrotoxicity	None	None	None
Applicability for wound dressing		Regular	Excellent	Unsuitable

SCT-CM, *Styela clava* tunic-cellulose membranes; FSCT-CM, freeze-dried SCT-CM; ASCT-CM, sodium alginate-supplemented SCT-CM; WVTR, water vapor transmission rate.

the two aforementioned studies, even though the results for the early stage differed.

The wound healing of skin may contribute to angiogenesis through the production of microvessels that transport nutrients and oxygen to growing dermal cells (36). Several functional extracts, including angico extract (*Anadenanthera colubrina* var. *cebil*) have been shown to induce a significant increase in the number of blood vessels during the healing of rat skin at 7 and 14 days post-surgery, although such an increase was not measured in the cellulose-treated animals (37). Alterations in the levels of VEGF, one of the major regulatory cytokines involved in angiogenesis, have been detected in surgical wound repair in skin. In a previous study, the group treated with HCM-SCT exhibited an 18.8% decrease in VEGF expression when compared with the GZ-treated group at 11 days post-surgery (11). Moreover, a decrease in the expression of VEGF was observed in the group treated with microbial cellulose on day 14 after skin excision, although it was higher in the same group on day 7 (38). In the present study, the number of blood vessels and the expression level of VEGF were higher in the FSCT-CM-treated group than the other groups on day 7, while their levels were lower on day 14. These results are in complete agreement with those of previous studies, although the relative ratio of increase or decrease differed.

Collagen is a key component of the extracellular matrix that plays an important role in all phases of surgical wound healing (39). The altered deposition of collagen has been observed in surgically wounded skin treated with several therapeutic compounds and SCT mixture. In a previous study, collagen deposition was higher in the dorsal incision wound treated with total ginseng saponin than in the control group (40). Moreover, the expression of collagen was upregulated significantly in the surgical skin wounds of rats treated with HCM-SCT on day 11 (11). In the present study, the expression of collagen was only higher in the FSCT-CM-treated group than the other groups on day 14, although a constant level was maintained on day 7. These results were similar to those of previous studies.

TGF-β1 signaling plays a crucial role in re-epithelialization, inflammation, angiogenesis and granulation tissue formation during wound healing (41). This signaling mediates their effects through both the Smad-dependent and Smad-independent pathway (20,42). The activation of the Smad-dependent pathway via stimulation with TGF-β1 can induce the synthesis and secretion of collagen, leading to increased scar formation (43,44). In addition, the concentration of TGF-β1 in serum has been shown to change in response to treatment with cellulose complex. Specifically, an approximately 266% increase in the TGF-β1 concentration was previously measured in SD rats treated with HCM-SCT on day 11 when compared to the GZ- or HCM-treated groups (11). The results of this study are in agreement with those of previous studies, although the

final analysis point and level of increase differed (Fig. 6). The correlation between the Smad-dependent pathway and cellulose wound dressing on healing has not been reported in any previous studies, at least to the best of our knowledge. In the present study, the expression of p-Smad2/3 in the FSCT-treated group was higher on days 7 and 14 than that of the GZ-treated group. Therefore, the present study provides novel evidence that FSCT-CM may accelerate the wound healing of surgically wounded skin through the regulation of the TGF-β1 signaling pathway.

Finally, several studies have suggested that SCT complexes and derivatives do not show any toxicity in mammalian systems. Specifically, SD rats treated with HCM-SCT for 11 days did not induce any specific toxicity based on body weight or metabolic enzymes of the liver and kidney (11). In addition, the concentration of metabolic enzymes representing liver and kidney toxicity in the serum of SCT-CF-treated SD rats was maintained at a constant level relative to the vehicle implanted group (14). In this study, most indicators of liver and kidney toxicity were maintained at a constant level in the three SCT-CM-treated groups throughout the experimental period. These results are in agreement with the finding that SCT derived materials were not correlated with animal toxicity.

Taken together, the results of our study demonstrated that the topical application of the three SCT-CMs for 2 weeks induced the acceleration of the healing of surgical wounds, including tissue regeneration, connective formation and angiogenesis. Among these, FSCT-CM exerted the greatest therapeutic effect on surgical wound healing of the back skin of SD rats. Moreover, this study provides insight into the molecular action of FSCT-CM in a rat model of surgical wound healing using SD rats (Table IV). Finally, this study demonstrated that the three SCT-CMs do not induce any significant toxicity toward the livers and kidneys of SD rats. Overall, our results provide a rationale for the future development of FSCT-CM with other functional compounds for topical application to cutaneous wounds.

Acknowledgements

This study was supported by a grant to Professor Dae Youn Hwang from the Korea Institute of Marine Science and Technology Promotion (112088-3). In addition, this manuscript was proofread and edited by Jeremy Kaman, one of the English editors at NURISCO (NU-150202).

References

1. Eaglstein WH: Moist wound healing with occlusive dressings: A clinical focus. Dermatol Surg 27: 175-181, 2001.
2. Mark GL, Warren RH, John BJ and Ian C: Treatment of skin disease: comprehensive therapeutic strategies. In: Decubitus Ulcers. 4th edition. Joseph AW, Lawrence CP, Caren C and Jennifer LP (eds). Elsevier Health Sciences, UK, pp167-171, 2013.
3. Kim JO, Choi JY, Park JK, Kim JH, Jin SG, Chang SW, Li DX, Hwang MR, Woo JS, Kim JA, *et al*: Development of clindamycin-loaded wound dressing with polyvinyl alcohol and sodium alginate. Biol Pharm Bull 31: 2277-2282, 2008.
4. Crépy L, Monchau F, Chai F, Raoul G, Hivart P, Hildebrand HF, Martin P and Joly N: Evaluation of a bio-based hydrophobic cellulose laurate film as biomaterial - study on biodegradation and cytocompatibility. J Biomed Mater Res B Appl Biomater 100: 1000-1008, 2012.
5. Thomas S: Wound Management and Dressing. Pharmaceutical Press, London, 1990.
6. Woodley DT, Chen JD, Kim JP, Sarret Y, Iwasaki T, Kim YH and O'Keefe EJ: Re-epithelialization. Human keratinocyte locomotion. Dermatol Clin 11: 641-646, 1993.
7. Jayakumar R, Prabaharan M, Sudheesh Kumar PT, Nair SV and Tamura H: Biomaterials based on chitin and chitosan in wound dressing applications. Biotechnol Adv 29: 322-337, 2011.
8. Witthayaprapakorn C: Design and preparation of synthetic hydrogels via photopolymerisation for biomedical uses as wound dressings. Procedia Eng 8: 286-291, 2011.
9. Yang JM and Lin HT: Properties of chitosan containing PP-g-AA-g-NIPAAm bigraft nonwoven fabric for wound dressing. J Membr Sci 243: 1-7, 2004.
10. Camargo MC, Nogueira RM, Sanches OC, Saab MG, Batista A, Vasconcelos D, Luvisotto LY and Lúcio MA: Applicability of crystalline cellulose membrane in the treatment of skin wounds induced in Wistar rats. Acta Cir Bras 29: 429-437, 2014.
11. Kwak MH, Go J, Kim JE, Lee YJ, Lee SH, Lee HS, Son HJ, Jung YJ and Hwang DY: Property and efficacy analysis of hydrocolloid membrane containing *Styela clava* tunic on the wound repair of skin in SD rats. Biomater Res 17: 91-101, 2013.
12. Hart J, Silcock D, Gunnigle S, Cullen B, Light ND and Watt PW: The role of oxidised regenerated cellulose/collagen in wound repair: Effects *in vitro* on fibroblast biology and *in vivo* in a model of compromised healing. Int J Biochem Cell Biol 34: 1557-1570, 2002.
13. Jung YJ: Properties of regenerated cellulose films prepared from the tunicate *Styela clava*. J Kor Fish Soc 41: 237-242, 2008.
14. Song SH, Kim JE, Lee YJ, Kwak MH, Sung GY, Kwon SH, Son HJ, Lee HS, Jung YJ and Hwang DY: Cellulose film regenerated from *Styela clava* tunics have biodegradability, toxicity and biocompatibility in the skin of SD rats. J Mater Sci Mater Med 25: 1519-1530, 2014.
15. Jung YJ, An BJ, Hwang DY, Kim HD, Park SM, Cho H and Kim HS: Preparation and properties of regenerated cellulosic biomaterial made from *Styela Clava* tunics. Biomater Res 12: 71-76, 2008.
16. Pereira RF, Mendes A and Bártolo PJ: Novel alginate/Aloe Vera hydrogel blends as wound dressings for the treatment of several types of wounds. Chem Eng Prog 32: 1009-1014, 2013.
17. ASTM standard E96-00. Standard test methods for water vapour transmission of materials.
18. Kim HJ, Kim J, Kim SJ, Lee SH, Park YS, Park BK, Kim BS, Kim SK, Cho SD, Jung JW, *et al*: Anti-inflammatory effect of Quercetin on picryl chloride-induced contact dermatitis in BALB/c mice. Lab Anim Res 26: 7-13, 2010.
19. Baum CL and Arpey CJ: Normal cutaneous wound healing: Clinical correlation with cellular and molecular events. Dermatol Surg 31: 674-686, 2005.
20. Derynck R and Zhang YE: Smad-dependent and Smad-independent pathways in TGF-beta family signalling. Nature 425: 577-584, 2003.
21. Yu L, Hébert MC and Zhang YE: TGF-beta receptor-activated p38 MAP kinase mediates Smad-independent TGF-beta responses. EMBO J 21: 3749-3759, 2002.
22. Matasuzaki K, Yamamoto I, Sato T and Oshima R: Synthesis of water-soluble branched polysaccharides and their antitumor activity, 1. Branched polysaccharides from cellulose acetate. Macromol Chem Phys 186: 449-456, 1985.
23. Ito H, Shibata T, Miyamoto T, Inagaki H and Noishiki Y: Formation of polyelectrolyte complexes between cellulose derivatives and their blood compatibility. J Appl Polym Sci 31: 2491-2500, 1986.
24. Hirano S: Chitin biotechnology applications. Biotechnol Annu Rev 2: 237-258, 1996.
25. Müller FA, Müller L, Hofmann I, Greil P, Wenzel MM and Staudenmaier R: Cellulose-based scaffold materials for cartilage tissue engineering. Biomaterials 27: 3955-3963, 2006.
26. Seong KY, Koh EK, Lee SH, Kwak MH, Son HJ, Lee HS, Hwang DY and Jung YJ: Preparation and characterization of high absorptive cellulose film derived from *Styela Clava* tunic for wound dressing. Text Coloration Finish 27: 70-79, 2015.
27. Zhang L, Ruan D and Gao S: Dissolution and regeneration of cellulose in NaOH/thiourea aqueous solution. J Polym Sci Pol Phys 40: 1521-1529, 2002.
28. Cheng Y, Lu J, Liu S, Zhao P, Lu G and Chen J: The preparation, characterization and evaluation of regenerated cellulose/collagen composite hydrogel films. Carbohydr Polym 107: 57-64, 2014.
29. Pang J, Liu X, Zhang X, Wu Y and Sun R: Fabrication of cellulose film with enhanced mechanical properties in ionic liquid 1-Allyl-3-methylimidaxolium chloride (AmimCl). Materials (Basel) 6: 1270-1284, 2013.

30. Queen D, Evans JH, Gaylor JDS, Courtney JM and Reid WH: An *in vitro* assessment of wound dressing conformability. Biomaterials 8: 372-376, 1987.
31. Mi FL, Shyu SS, Wu YB, Lee ST, Shyong JY and Huang RN: Fabrication and characterization of a sponge-like asymmetric chitosan membrane as a wound dressing. Biomaterials 22: 165-173, 2001.
32. Wu P, Fisher AC, Foo PP, Queen D and Gaylor JD: *In vitro* assessment of water vapour transmission of synthetic wound dressings. Biomaterials 16: 171-175, 1995.
33. Ulrich D, Smeets R, Unglaub F, Wöltje M and Pallua N: Effect of oxidized regenerated cellulose/collagen matrix on proteases in wound exudate of patients with diabetic foot ulcers. J Wound Ostomy Continence Nurs 38: 522-528, 2011.
34. Trabucchi E, Radaelli E, Marazzi M, Foschi D, Musazzi M, Veronesi AM and Montorsi W: The role of mast cells in wound healing. Int J Tissue React 10: 367-372, 1988.
35. Liu SA, Cheng CC, Chen JS, Hung YW, Chen FJ and Chiu YT: Effect of oxidized regenerated cellulose on the healing of pharyngeal wound: An experimental animal study. J Chin Med Assoc 75: 176-182, 2012.
36. Andrikopoulou E, Zhang X, Sebastian R, Marti G, Liu L, Milner SM and Harmon JW: Current Insights into the role of HIF-1 in cutaneous wound healing. Curr Mol Med 11: 218-235, 2011.
37. Pessoa WS, Estevão LR, Simões RS, Barros ME, Mendonça FS, Baratella-Evêncio L and Evêncio-Neto J: Effects of angico extract (*Anadenanthera colubrina var. cebil*) in cutaneous wound healing in rats. Acta Cir Bras 27: 655-670, 2012.
38. Park SU, Lee BK, Kim MS, Park KK, Sung WJ, Kim HY, Han DG, Shim JS, Lee YJ, Kim SH, *et al*: The possibility of microbial cellulose for dressing and scaffold materials. Int Wound J 11: 35-43, 2014.
39. Mian M, Beghè F and Mian E: Collagen as a pharmacological approach in wound healing. Int J Tissue React 14 (Suppl): 1-9, 1992.
40. Kim YS, Cho IH, Jeong MJ, Jeong SJ, Nah SY, Cho YS, Kim SH, Go A, Kim SE, Kang SS, *et al*: Therapeutic effect of total ginseng saponin on skin wound healing. J Ginseng Res 35: 360-367, 2011.
41. Ramirez H, Patel SB and Pastar I: The role of TGFβ signaling in wound epithelialization. Adv Wound Care (New Rochelle) 3: 482-491, 2014.
42. Willis BC, Borok Z and Am J: TGF-beta-induced EMT: Mechanisms and implications for fibrotic lung disease. Am J Physiol Lung Cell Mol Physiol 293: L525-L534, 2007.
43. Ihn H: Autocrine TGF-beta signaling in the pathogenesis of systemic sclerosis. J Dermatol Sci 49: 103-113, 2008.
44. Qi SH, Xie JL, Pan S, Xu YB, Li TZ, Tang JM, Liu XS, Shu B and Liu P: Effects of asiaticoside on the expression of Smad protein by normal skin fibroblasts and hypertrophic scar fibroblasts. Clin Exp Dermatol 33: 171-175, 2008.